

# Tb(HSO<sub>4</sub>)(SO<sub>4</sub>) – a green emitting hydrogensulfate sulfate with second harmonic generation response†

Philip Netzsch,<sup>a</sup> Harijs Bariss,<sup>a</sup> Lkhamsuren Bayarjargal<sup>b</sup> and Henning A. Höppe<sup>a\*</sup>

Recently, sulfates have attracted attention as materials for non-linear optical applications. This compound class is extended by Tb(HSO<sub>4</sub>)(SO<sub>4</sub>), which is solvothermally synthesised from Tb<sub>4</sub>O<sub>7</sub> and sulfuric acid. The compound crystallises in the non-centrosymmetric space group *P*2<sub>1</sub> (*Z* = 2, *a* = 665.03(5) pm, *b* = 659.41(5) pm, *c* = 680.24(5) pm, and *β* = 104.640(2)°) and is homeotypic with Ni<sub>2</sub>In. The terbium ions adopt the indium sites and the sulfate and hydrogen sulfate anions are situated on the nickel sites. The compound shows green luminescence based on f–f-transitions and the positions of the f–d-excitation bands reveal a weak coordination behaviour of the sulfate anions. Tb(HSO<sub>4</sub>)(SO<sub>4</sub>) exhibits a second harmonic generation response comparable to KH<sub>2</sub>PO<sub>4</sub> (KDP). Furthermore, the material is characterised by electrostatic calculations, infrared spectroscopy and thermal analysis.

## Introduction

Non-linear optical (NLO) materials have attracted great attention due to their properties of frequency doubling based on the second harmonic generation (SHG) effect. A compulsory requirement for those materials is a non-centrosymmetric crystal structure, *i.e.* the lack of an inversion centre.<sup>1</sup> In recent years, researchers have focussed mainly on borates due to their suitable properties, yielding compounds like β-BaB<sub>2</sub>O<sub>4</sub> (BBO),<sup>2</sup> LiB<sub>3</sub>O<sub>5</sub> (LBO),<sup>3</sup> or Sr<sub>2</sub>Be<sub>2</sub>B<sub>2</sub>O<sub>7</sub> (SBBO).<sup>4</sup> In order to increase the polarizability of the borate backbone as well as the bandgap, the oxygen atoms were partially substituted by fluorine atoms leading to the so-called compound class of fluorooxoborates, with KBe<sub>2</sub>BO<sub>3</sub>F<sub>2</sub> (KBBF),<sup>5</sup> BiB<sub>2</sub>O<sub>4</sub>F<sup>6</sup> and Sn[B<sub>2</sub>O<sub>3</sub>F<sub>2</sub>]<sup>7,8</sup> as typical NLO representatives. Besides, further silicate-analogous materials, *i.e.* compounds comprising non-centrosymmetric tetrahedral building units like the phosphates LiFeP<sub>2</sub>O<sub>7</sub>,<sup>9</sup> Ba<sub>3</sub>P<sub>3</sub>O<sub>10</sub>X (*X* = Cl, Br)<sup>10</sup> and LiGaP<sub>2</sub>O<sub>7</sub>,<sup>11</sup> showed promising NLO properties.

Very recently, sulfates with analogous non-π conjugated [SO<sub>4</sub>]<sup>2-</sup> groups have gained interest as potential NLO materials.<sup>12</sup> As a result, several representatives with

remarkable SHG response like LiNa(SO<sub>4</sub>)<sub>2</sub>·H<sub>2</sub>O,<sup>13</sup> Li<sub>8</sub>NaRb<sub>3</sub>(SO<sub>4</sub>)<sub>6</sub>·H<sub>2</sub>O,<sup>14</sup> (NH<sub>4</sub>)Sb(SO<sub>4</sub>)Cl<sub>2</sub>,<sup>15</sup> CsSbF<sub>2</sub>(SO<sub>4</sub>),<sup>16</sup> Nb<sub>2</sub>O<sub>3</sub>(IO<sub>3</sub>)<sub>2</sub>(SO<sub>4</sub>),<sup>17</sup> NH<sub>4</sub>NaLi<sub>2</sub>SO<sub>4</sub>,<sup>12</sup> RbSbSO<sub>4</sub>Cl<sub>2</sub>,<sup>18</sup> and A<sub>2</sub>Bi<sub>2</sub>(SO<sub>4</sub>)<sub>2</sub>Cl<sub>4</sub><sup>19</sup> (*A* = NH<sub>4</sub>, K, Rb) were presented. However, in Nb<sub>2</sub>O<sub>3</sub>(IO<sub>3</sub>)<sub>2</sub>(SO<sub>4</sub>), for example, the SHG effect is mainly based on the NbO<sub>6</sub> units,<sup>17</sup> whereas in Li<sub>8</sub>NaRb<sub>3</sub>(SO<sub>4</sub>)<sub>6</sub>·H<sub>2</sub>O the effect can be attributed to the sulfate tetrahedra.<sup>14</sup> In order to increase the impact of the sulfate anions, a higher polarity, *e.g.*, of heteroleptic tetrahedra should be addressed.<sup>20</sup> One approach might be the protonation of an oxygen atom within the sulfate tetrahedra leading to a hydroxyl group with a longer S–O bond. A mixed sulfate hydrogen sulfate with a non-centrosymmetric space group is Th<sub>4</sub>(HSO<sub>4</sub>)<sub>2</sub>(SO<sub>4</sub>)<sub>7</sub>.<sup>21</sup> Referring to rare earth compounds, only the structures of Er(SO<sub>4</sub>)(HSO<sub>4</sub>)<sup>22</sup> and (H<sub>3</sub>O)<sub>2</sub>Nd(HSO<sub>4</sub>)<sub>3</sub>SO<sub>4</sub><sup>23</sup> are known, both crystallising in centrosymmetric space groups. In this context, the non-centrosymmetric lanthanide hydroxide sulfate hydrates Ln<sub>4</sub>(OH)<sub>4</sub>(SO<sub>4</sub>)<sub>4</sub>(H<sub>2</sub>O)<sub>3</sub> (*Ln* = Y, Er) are worth mentioning.<sup>24</sup> Here, the chiral compound—mainly originating from the helical chains of condensed lanthanide sulfate moieties—could only be obtained using a crystallisation agent not present in the crystal structure. Generally, there are only limited amounts of characterised anhydrous rare earth sulfates, due to their difficult crystallisation.<sup>25</sup> Several pure hydrogen sulfates were synthesised,<sup>22,26–28</sup> whereas pure sulfates of trivalent lanthanides are limited to RE<sub>2</sub>(SO<sub>4</sub>)<sub>3</sub> (*RE* = Sc, Y, Nd, Er, Yb, Lu).<sup>22,29–31</sup> Therefore, little is known of the optical properties of such compounds, *i.e.* neither absorption spectra nor luminescence spectra have been obtained so far. The herein reported Tb(HSO<sub>4</sub>)(SO<sub>4</sub>) adopting the non-centrosymmetric

<sup>a</sup>Chair of Solid State and Materials Chemistry, University of Augsburg, Universitätsstraße 1, D-86159 Augsburg, Germany. E-mail: henning@ak-hoeppe.de

<sup>b</sup>Institut für Geowissenschaften, Universität Frankfurt, Altenhöferallee 1, D-60438 Frankfurt, Germany

† Electronic supplementary information (ESI) available. CCDC 1923048. For ESI and crystallographic data in CIF or other electronic format see DOI: 10.1039/C9DT03436F

space group  $P2_1$  broadens the field of NLO-active sulfates and furthermore gives insights into the coordination behaviour of sulfates based on their optical spectra.

## Experimental section

### Synthesis

Tb(HSO<sub>4</sub>)(SO<sub>4</sub>) was synthesised under solvothermal conditions, by loading 0.1239 g (0.166 mmol) of Tb<sub>4</sub>O<sub>7</sub> together with 2.5 mL of conc. H<sub>2</sub>SO<sub>4</sub> into a silica glass ampule. In addition, 0.3 mL of oleum (65% SO<sub>3</sub>) was added, as this route provided the highest crystal quality. After torch sealing, the ampule was placed in a furnace and heated up to 300 °C within 3 h. After 96 h, the temperature was decreased to room temperature at a rate of 50 °C h<sup>-1</sup>. Solely colourless single crystals were formed and the yield was almost quantitative with respect to Tb<sub>4</sub>O<sub>7</sub>. Phase purity was checked *via* powder diffraction (Fig. 1). The ampules were opened after cooling down with liquid nitrogen. The bulk excess of the acid was pipetted, whereas the adhesive acid was evaporated at 300 °C. The crystals are sensitive to moisture and hence are stored under inert conditions.

### Crystal structure determination

Immediately after opening the ampule, the single-crystals were transferred into perfluorinated polyether and selected for single-crystal XRD. Diffraction data for all compounds were collected with a Bruker D8 Venture diffractometer using Mo-K<sub>α</sub> radiation ( $\lambda = 0.71073 \text{ \AA}$ ). Absorption correction was done by the multi-scan method and then the crystal structure was solved by direct methods and refined by the full-matrix least-squares technique within the SHELXTL program.<sup>32</sup> The structure was refined as an inversion twin.

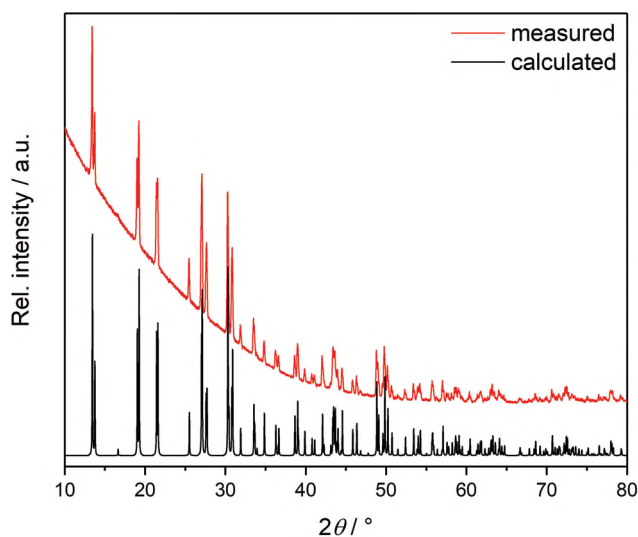


**Fig. 1** The PXRD pattern of Tb(HSO<sub>4</sub>)(SO<sub>4</sub>) (red) in comparison to the calculated pattern derived from single-crystal data (black).

Further details of the crystal structure determination are listed in Table 3 as well as in Tables S1 and S2 of the ESI.†

### X-ray powder diffraction

The sample was ground and filled into a Hilgenberg glass capillary (outer diameter 0.3 mm and wall thickness 0.01 mm) inside a glove box. The data were collected with a Bruker D8 Advance diffractometer equipped with a Cu-K<sub>α</sub> radiation source ( $\lambda = 1.54184 \text{ \AA}$ ) and a 1D LynxEye detector.

### Infrared spectroscopy

The infrared spectrum was recorded using a Bruker EQUINOX 55 FT-IR spectrometer equipped with a platinum ATR setup in the range of 4000–400 cm<sup>-1</sup>.

### UV/VIS spectroscopy

The optical reflection spectrum was measured with a Varian Cary 300 Scan UV/vis spectrophotometer in the range of 200–800 nm.

### Fluorescence spectroscopy

Solid-state excitation and emission spectra were recorded at room temperature using a Horiba FluoroMax-4 fluorescence spectrometer equipped with a xenon discharge lamp scanning a range from 200 to 800 nm. The excitation spectrum was corrected with respect to the lamp intensity.

### SHG measurements

Second harmonic generation (SHG) measurements were performed on a powder sample of Tb(HSO<sub>4</sub>)(SO<sub>4</sub>). A Q-switched Nd:YAG laser (1064 nm, 5–6 ns, 2 kHz) was used for the generation of the fundamental pump wave. With a harmonic separator, a short-pass filter, and an interference filter, the fundamental infrared light was separated from the generated second harmonics (532 nm). The generated SHG signal was collected on ten different areas of the sample to check its homogeneity. On each position 64 pulses were measured and averaged. The measured intensities were background-corrected by signals collected between the laser pulses. As reference materials Al<sub>2</sub>O<sub>3</sub>, quartz, KDP (KH<sub>2</sub>PO<sub>4</sub>) were used.

### Thermal analysis

Thermogravimetric analysis was done in alumina crucibles employing an NETZSCH STA 409 PC Luxx in synthetic air (20% O<sub>2</sub>; 80% N<sub>2</sub>) and a heating ramp of 10 °C min<sup>-1</sup>.

## Results and discussion

### Crystal structure

Tb(HSO<sub>4</sub>)(SO<sub>4</sub>) crystallises in a new structure type in the non-centrosymmetric space group  $P2_1$  with two formula units per unit cell (Fig. 2). The structure is homeotypic with Ni<sub>2</sub>In,<sup>33</sup> where terbium ions form a distorted *hcp* lattice and occupy the In sites. The hexagonal angle is decreased to a monoclinic angle of 104.640(2)°. The sulfate and hydrogensulfate sites

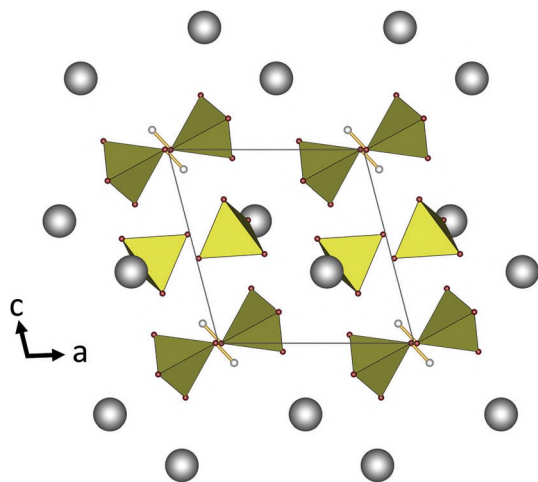


Fig. 2 The crystal structure of  $\text{Tb}(\text{HSO}_4)(\text{SO}_4)$  along [010]; sulfate tetrahedra yellow, Tb cations grey, and H ions light grey.

substitute the Ni atoms. Thus, the protonated oxygen atoms of the hydrogen sulfate anions are situated in all octahedral voids, with the corresponding anion slightly shifted out of the centre. The sulfate anions occupy all trigonal bipyramidal voids (Fig. 4). A comparison of the crystal structures of  $\text{Ni}_2\text{In}$  and the reduced substructure (O)(S)Tb (O: protonated oxygen of the hydrogensulfate anion and S: sulfur of the sulfate tetrahedron) is displayed in Fig. 3; the symmetry relation can be understood by a group-subgroup scheme according to the Bärnighausen formalism (Fig. S1†).<sup>34</sup>

Both tetrahedra can be classified as regular as the deviation from the tetrahedral symmetry<sup>35,36</sup> amounts to 0.24% ( $\text{S}_2\text{O}_4^{2-}$ ) and 0.05% ( $\text{S}_1\text{O}_4^-$ ), respectively. The S–O bonds in the sulfate anion range between 145.3(5) and 150.0(5) pm, whereas the

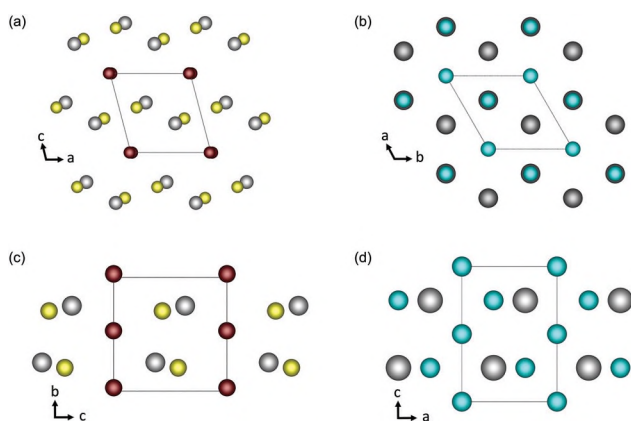


Fig. 3 The crystal structure of  $\text{Tb}(\text{HSO}_4)(\text{SO}_4)$ , along [010] (a) and [100] (c) and as a comparison the structure of  $\text{Ni}_2\text{In}$  along [001] (b) and [010] (d). For a better understanding, only the sulfur atoms of the sulfate and the protonated oxygen atom of the hydrogen sulfate tetrahedra are displayed. Terbium atoms are grey spheres, sulfur atoms yellow, oxygen atoms red, indium atoms are dark grey spheres and nickel atoms turquoise spheres.

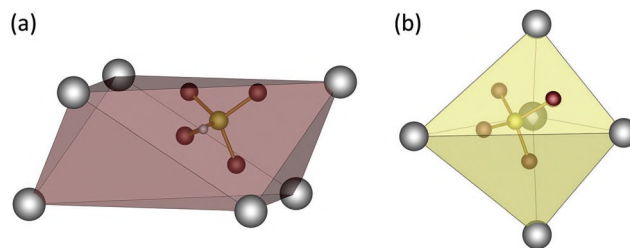


Fig. 4 (a) Hydrogen sulfate ions in the octahedral void and (b) sulfate ions in the trigonal bipyramidal void of the distorted cationic hcp lattice.

oxygen with the longest bond coordinates to two terbium cations. The hydrogen sulfate anion exhibits three short S–O bonds between 144.5(4) and 145.4(5) pm and an elongated S–O bond of length 152.6(8) pm with the hydrogenated oxygen atom. Furthermore, this oxygen atom does not coordinate to a terbium cation, which clearly indicates the OH-group (Fig. 5). The bond lengths are in good agreement with other sulfates and hydrogensulfates.<sup>21,22,26,27,37,38</sup> The sulfate and hydrogen sulfate anions form pairs *via* a connecting hydrogen bond. The acceptor hydrogen distance amounts to 171.1 pm, the donor (D)–acceptor (A) distance amounts to 263.2 pm and the bond angle  $\angle(\text{DHA})$  is 169.7°. Thus, the hydrogen bond can be classified as moderate.<sup>39</sup> The terbium cations are coordinated by one bidentate sulfate, three monodentate sulfate and three monodentate hydrogen sulfate anions in a distorted square antiprism (Fig. 6). Hence, according to  $\text{Tb}(\text{HSO}_4)_{3/3}(\text{SO}_4)_{4/4}$  a three dimensional framework is formed (Fig. S2†). The Tb–O bonds range between 230.4(5) and 253.4(5) pm and are within the sum of the ionic radii ( $\sum r_{\text{ion}} = 239$  pm).<sup>40</sup>

### Electrostatic calculations

The crystal structure was checked for electrostatic consistency by calculations based on the MAPLE concept (Madelung Part of the Lattice Energy).<sup>41–43</sup> Therefore, the MAPLE values of  $\text{Tb}(\text{OH})\text{SO}_4$ <sup>44</sup> and  $\text{SO}_3$ <sup>45</sup> were calculated and the sum was com-

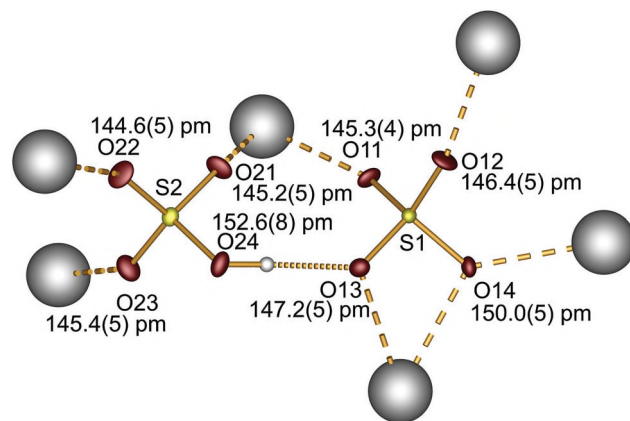


Fig. 5 The coordination environment, the hydrogen bond and the interatomic S–O distances of the sulfate and hydrogen sulfate tetrahedra; ellipsoids of sulfur and oxygen atoms are set to 70% probability.

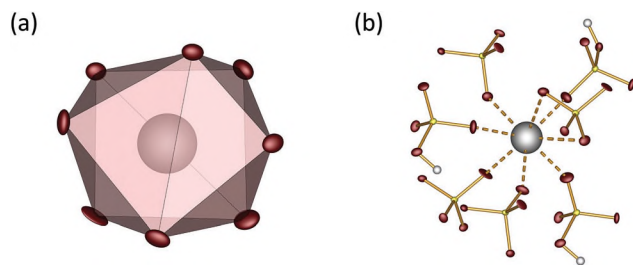


Fig. 6 (a) The distorted quadratic antiprismatic coordination environment of  $Tb^{3+}$  and (b) the enlarged coordination environment.

Table 1 Calculated MAPLE values for  $Tb(HSO_4)(SO_4)$  and the sum of  $Tb(OH)(SO_4)$  and  $SO_3$

$Tb(HSO_4)(SO_4)$	$Tb(OH)SO_4 + SO_3$
MAPLE = 70 858 $kJ\ mol^{-1}$	MAPLE = 70 506 $kJ\ mol^{-1}$
$\Delta = 0.5\%$	

pared to  $Tb(HSO_4)(SO_4)$  (Table 1). Since the deviation remains below 1% the structure can be considered as electrostatically consistent. In addition, the calculations confirmed the coordination number of eight for terbium (Table S3†).

### Vibrational spectroscopy

The infrared spectrum of  $Tb(HSO_4)(SO_4)$  is depicted in Fig. 7. The bands at 426 and 435  $cm^{-1}$  can be assigned to the symmetric bending vibrations of the sulfate and hydrogen sulfate tetrahedra. The bands between 494 and 660  $cm^{-1}$  correspond to asymmetric bending vibrations. Symmetric stretching vibrations are at 949 and 1001  $cm^{-1}$ . The bands between 1051 and 1246  $cm^{-1}$  can be assigned to the asymmetric stretching vibrations. Furthermore, the weak band at 1305  $cm^{-1}$  corresponds to the OH-bending vibration of the hydrogen sulfate

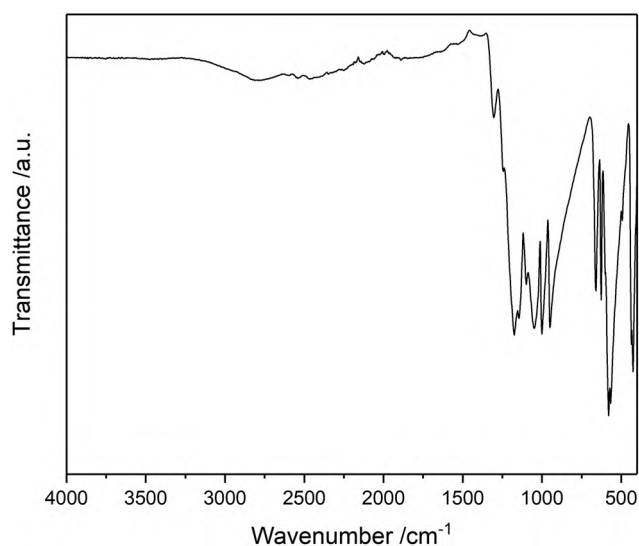


Fig. 7 The infrared spectrum of  $Tb(HSO_4)(SO_4)$ .

anion, whereas the stretching vibrations of the OH group appear as a broad band at around 2700  $cm^{-1}$ .<sup>37,46,47</sup>

### Second harmonic generation measurements

The SHG properties of the  $Tb(HSO_4)(SO_4)$  sample were investigated using the powder SHG method developed by Kurtz and Perry.<sup>48</sup> This method is commonly used as a first step to estimate the nonlinear optical properties of new materials or to detect the absence of an inversion centre in crystalline structures.

Table 2 shows the intensity of the SHG signal of the sample in comparison to several reference compounds ( $Al_2O_3$ , quartz, and KDP). The ratio of the sample signal and the reference signal provides an estimation of the effective SHG coefficient. The SHG intensity of  $Tb(HSO_4)(SO_4)$  was around 347 mV, which is  $\sim 11$  times higher than the intensity of quartz and comparable to the intensity of KDP. This strong SHG signal

Table 2 SHG intensities of quartz, KDP,  $Al_2O_3$ ,  $Tb(HSO_4)(SO_4)$  and Markröhrcchen (sample container) and their relative intensities with respect to quartz

Samples	SHG intensity/mV	$I_{SHG}/I_{quartz}$
Quartz	31.0(9.9)	1
KDP ( $KH_2PO_4$ )	296.9(31.1)	9.58
$Al_2O_3$	0.2(0.2)	0.006
$Tb(HSO_4)(SO_4)$	347.4(159.8)	11.2
Markröhrcchen	0.2(0.2)	0.006

Table 3 Crystal data and details of the structure refinements for  $Tb(HSO_4)(SO_4)$ ; the standard deviations are given in parentheses

Temperature/K	250(2)
Molar weight/ $g\ mol^{-1}$	352.05
Crystal system	Monoclinic
Space group	$P2_1$
Crystal shape	Block
Colour	Colourless
$a/pm$	665.03(5)
$b/pm$	659.41(5)
$c/pm$	680.24(5)
$\beta/^\circ$	104.640(2)
Volume/ $10^6\ pm^3$	288.62(4)
$Z$	2
Calculated density $D_x/g\ cm^{-3}$	4.051
Absorption coefficient $\mu/mm^{-1}$	12.975
$F(000)$	324
Radiation ( $\lambda/\text{\AA}$ )	0.71073
Diffractometer	Bruker D8 Venture
Absorption correction	Multi-scan
Transmission factor (min/max)	0.6057/0.7462
Index range $h k l$ (min/max)	-9/9 -9/9 -9/9
Theta range/ $^\circ$	$3.095 < \theta < 31.166$
Reflections collected	7319
Independent reflections	1877
Observed reflections ( $I > 2\sigma$ )	1748
$R_{int}$	0.0491
Refined parameters	104
$R_1$ (all data)	0.0250
$wR_2$ (all data)	0.0358
Goof	0.926
Residual electron density (min/max)/ $e^- \text{\AA}^{-3}$	-0.859/0.925
BASF	0.032(17)

indicates that the sample  $\text{Tb}(\text{HSO}_4)(\text{SO}_4)$  clearly crystallises in a non-centrosymmetric space group. KDP is phase matchable and has a low effective SHG coefficient. Therefore, the sample can be phase matchable or non-matchable with a high SHG coefficient. The grain size dependence of SHG signals was not studied.

### UV/VIS spectroscopy

The UV/vis spectrum is depicted in Fig. 8. Several f-f-transitions originating from the ground state  $^7F_6$  are visible and assigned to the respective energy states of  $\text{Tb}^{3+}$ .<sup>49</sup> Furthermore a 4f-5d-transition arises at 257 nm.

### Fluorescence spectroscopy

The presence of the rare earth ion  $\text{Tb}^{3+}$  enables fluorescence spectroscopy and hence the investigation of the scarcely explored compound class of hydrogen sulfate sulfate (Fig. 9). The emission shows four bands originating from  $^5D_4 \rightarrow ^7F_J$  ( $J = 6, 5, 4, 3$ ).<sup>49</sup> The visible green luminescence is based on the dominating  $^5D_4 \rightarrow ^7F_5$  transition, as it has the largest probability of electric- and magnetic-dipole induced transitions.<sup>50</sup> In contrast, the transitions from the  $^5D_3$  state are completely suppressed due to cross-relaxation processes ( $^5D_3(\text{Tb}^{3+}) + ^7F_6(\text{Tb}^{3+}) \rightarrow ^5D_4(\text{Tb}^{3+}) + ^7F_0(\text{Tb}^{3+})$ ). The excitation spectrum reveals several sharp 4f-4f-transitions originating from the ground state  $^7F_6$ .<sup>49</sup> Besides, two parity allowed and spin-forbidden 4f-5d transitions occur at 224 and 258 nm. These high energy values indicate a rather weak ligand field splitting and hence a rather weak coordination behaviour of the sulfate and hydrogen sulfate ligands. These values are in the range of other weakly coordinating host structures like  $\text{Tb}_2[\text{B}_2(\text{SO}_4)_6]$  (212 and 254 nm)<sup>51</sup> or  $\text{YF}_3 : \text{Tb}^{3+}$  (215 and 255 nm).<sup>52</sup>

### Thermal analysis

The thermal stability of the title compound was investigated under synthetic air (Fig. 10) where the decomposition starts at

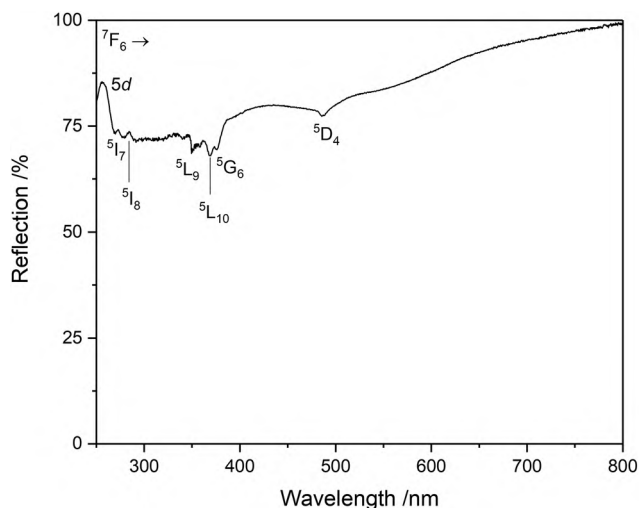


Fig. 8 The UV/vis spectrum of  $\text{Tb}(\text{HSO}_4)(\text{SO}_4)$ .

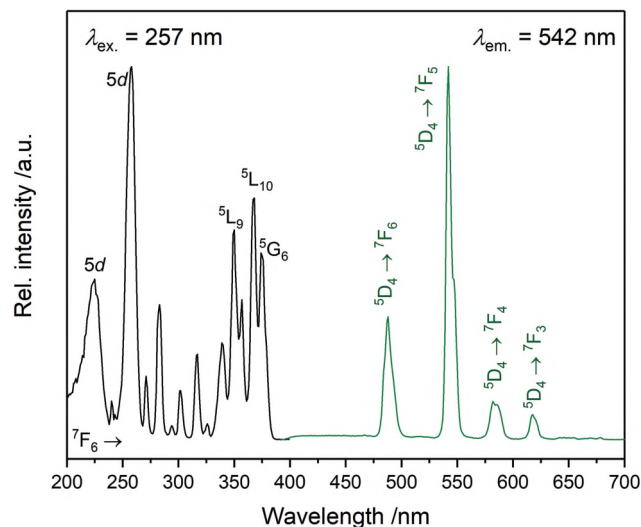


Fig. 9 Corrected excitation (black) and emission (green) spectra of  $\text{Tb}(\text{HSO}_4)(\text{SO}_4)$ ; complete assignment in Fig. S3 and Table S4.†

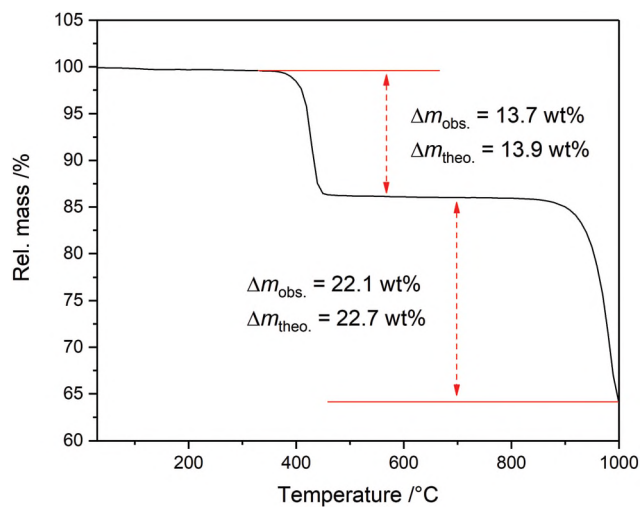


Fig. 10 Thermogravimetric analysis of  $\text{Tb}(\text{HSO}_4)(\text{SO}_4)$  under synthetic air (heating rate:  $10 \text{ K min}^{-1}$ ).

around  $350 \text{ }^\circ\text{C}$  with a maximum at  $429 \text{ }^\circ\text{C}$ . The observed mass loss of  $\Delta m_{\text{obs.}} = 13.7 \text{ wt}\%$  corresponds well to one mole of  $\text{SO}_3$  and one mole of  $\text{H}_2\text{O}$  per two moles of  $\text{Tb}(\text{HSO}_4)(\text{SO}_4)$  ( $\Delta m_{\text{theo.}} = 13.7 \text{ wt}\%$ ) resulting theoretically in  $\text{Tb}_2(\text{SO}_4)_3$ :



A second decomposition step occurs with a maximum at  $979 \text{ }^\circ\text{C}$  and an observed mass loss of  $\Delta m_{\text{obs.}} = 22.1 \text{ wt}\%$ . This is in accordance with the decomposition to  $\text{Tb}_2\text{O}_2(\text{SO}_4)_3$  (Fig. S4†),<sup>53</sup> accompanied by the evolution of two moles of  $\text{SO}_3$  ( $\Delta m_{\text{theo.}} = 22.7 \text{ wt}\%$ ), which presumably further decompose into  $\text{SO}_2$  and  $\text{O}_2$  under these conditions.



Due to the absence of crystal water, the compound shows higher thermal stability than the NLO active sulfates  $\text{LiNa}(\text{SO}_4)_2 \cdot \text{H}_2\text{O}$  ( $T_{\text{decomp.}} = 81\text{ }^\circ\text{C}$ , nitrogen atmosphere) or  $\text{Li}_3\text{NaRb}_3(\text{SO}_4)_6 \cdot \text{H}_2\text{O}$  ( $T_{\text{decomp.}} = 165\text{ }^\circ\text{C}$ , nitrogen atmosphere).

## Conclusions

We presented a new non-centrosymmetric sulfate, namely  $\text{Tb}(\text{HSO}_4)(\text{SO}_4)$ . The crystal structure is homeotypic with  $\text{Ni}_2\text{In}$ . Herein, the  $\text{Tb}^{3+}$  ions are related to In and form a distorted *hcp* packing, whereas the sulfate and hydrogen sulfate tetrahedra occupy all octahedral and trigonal bipyramidal voids corresponding to the Ni sites.

Within this contribution, we focussed on both the fluorescence spectroscopy of the optically active rare earth ion and the corresponding coordination behaviour of the sulfate host, as well as on the SHG properties based on the non-centrosymmetric space group  $P2_1$ . The green emission of the title compound originates mainly from the  ${}^5\text{D}_4 \rightarrow {}^7\text{F}_5$  transition. The high energy position of the 5d states revealed a weak coordination behaviour comparable to the weakly coordinating borosulfate  $\text{Tb}_2[\text{B}_2(\text{SO}_4)_6]$ . The SHG experiments confirmed the absence of an inversion centre and thus the non-centrosymmetric space group.  $\text{Tb}(\text{HSO}_4)(\text{SO}_4)$  exhibits a SHG response, approximately 11 times that of quartz and comparable to KDP.

Focussing on the SHG properties, further research will utilize optically silent rare earth metals like  $\text{Y}^{3+}$ ,  $\text{La}^{3+}$ , or  $\text{Lu}^{3+}$  in order to achieve a potential deep UV NLO material.

## Conflicts of interest

There are no conflicts to declare.

## Acknowledgements

P. N. thanks the Fonds der Chemischen Industrie (FCI) for a Ph.D. fellowship.

## Notes and references

- 1 T. T. Tran, H. Yu, J. M. Rondinelli, K. R. Poeppelmeier and P. S. Halasyamani, *Chem. Mater.*, 2016, **28**, 5238–5258.
- 2 C. T. Chen, B. C. Wu, A. D. Jiang and G. M. You, *Sci. Sin., Ser. B*, 1985, **28**, 235.
- 3 C. Chen, Y. Wu, A. Jiang, B. Wu, G. You, R. Li and S. Lin, *J. Opt. Soc. Am. B*, 1989, **6**, 616.
- 4 C. Chen, Y. Wang, B. Wu, K. Wu, W. Zeng and L. Yu, *Nature*, 1995, **373**, 322–324.
- 5 L. Mei, Y. Wang, C. Chen and B. Wu, *J. Appl. Phys.*, 1993, **74**, 7014–7015.
- 6 R. Cong, Y. Wang, L. Kang, Z. Zhou, Z. Lin and T. Yang, *Inorg. Chem. Front.*, 2015, **2**, 170–176.
- 7 S. G. Jantz, M. Dialer, L. Bayarjargal, B. Winkler, L. van Wüllen, F. Pielhofer, J. Brgoch, R. Weihrich and H. A. Höpfe, *Adv. Opt. Mater.*, 2018, **6**, 1800497.
- 8 M. Luo, F. Liang, Y. Song, D. Zhao, N. Ye and Z. Lin, *J. Am. Chem. Soc.*, 2018, **140**, 6814–6817.
- 9 W. Zhang and P. S. Halasyamani, *Cryst. Growth Des.*, 2012, **12**, 2127–2132.
- 10 P. Yu, L.-M. Wu, L.-J. Zhou and L. Chen, *J. Am. Chem. Soc.*, 2014, **136**, 480–487.
- 11 Y. Li, F. Liang, H. Song, W. Liu, Z. Lin, G. Zhang and Y. Wu, *Inorg. Chem.*, 2019, **58**, 6597–6600.
- 12 Y. Li, F. Liang, S. Zhao, L. Li, Z. Wu, Q. Ding, S. Liu, Z. Lin, M. Hong and J. Luo, *J. Am. Chem. Soc.*, 2019, **141**, 3833–3837.
- 13 R. Punniyamoorthy, R. Manimekalai and G. Pasupathi, *Cryst. Res. Technol.*, 2018, **53**, 1800114.
- 14 Y. Li, S. Zhao, P. Shan, X. Li, Q. Ding, S. Liu, Z. Wu, S. Wang, L. Li and J. Luo, *J. Mater. Chem. C*, 2018, **6**, 12240–12244.
- 15 F. He, Q. Wang, C. Hu, W. He, X. Luo, L. Huang, D. Gao, J. Bi, X. Wang and G. Zou, *Cryst. Growth Des.*, 2018, **18**, 6239–6247.
- 16 X. Dong, L. Huang, C. Hu, H. Zeng, Z. Lin, X. Wang, K. M. Ok and G. Zou, *Angew. Chem., Int. Ed.*, 2019, **58**, 6528–6534.
- 17 H.-X. Tang, Y.-X. Zhang, C. Zhuo, R.-B. Fu, H. Lin, Z.-J. Ma and X.-T. Wu, *Angew. Chem., Int. Ed.*, 2019, **58**, 3824–3828.
- 18 F. He, Y. Deng, X. Zhao, L. Huang, D. Gao, J. Bi, X. Wang and G. Zou, *J. Mater. Chem. C*, 2019, **7**, 5748–5754.
- 19 K. Chen, Y. Yang, G. Peng, S. Yang, T. Yan, H. Fan, Z. Lin and N. Ye, *J. Mater. Chem. C*, 2019, **7**, 9900–9907.
- 20 M. Valldor, *Inorganics*, 2016, **4**, 23.
- 21 U. Betke and M. S. Wickleder, *Eur. J. Inorg. Chem.*, 2012, 306–317.
- 22 M. S. Wickleder, *Z. Anorg. Allg. Chem.*, 1998, **624**, 1347–1354.
- 23 M. S. Wickleder, *Z. Anorg. Allg. Chem.*, 1999, **625**, 474–480.
- 24 W.-H. Wang, H.-R. Tian, Z.-C. Zhou, Y.-L. Feng and J.-W. Cheng, *Cryst. Growth Des.*, 2012, **12**, 2567–2571.
- 25 M. S. Wickleder, *Chem. Rev.*, 2002, **102**, 2011–2088.
- 26 M. S. Wickleder, *Z. Anorg. Allg. Chem.*, 1999, **625**, 1707–1711.
- 27 M. S. Wickleder, *Z. Anorg. Allg. Chem.*, 1998, **624**, 1583–1587.
- 28 H.-U. Hummel, P. Joeg, G. Pezzeri and A. Wolski, *Z. Naturforsch., B: J. Chem. Sci.*, 1994, **49**, 347–349.
- 29 S. P. Sirotkin, V. A. Efremov, L. M. Kovba and A. N. Pokrovskii, *Kristallografiya*, 1977, **22**, 1272–1273.
- 30 S. J. Mills, V. Petříček, A. R. Kampf, R. Herbst-Imer and M. Raudsepp, *J. Solid State Chem.*, 2011, **184**, 2322–2328.
- 31 M. S. Wickleder, *Z. Anorg. Allg. Chem.*, 2000, **626**, 1468–1472.
- 32 G. M. Sheldrick, *Acta Crystallogr., Sect. A: Found. Crystallogr.*, 2008, **64**, 112–122.
- 33 F. Laves and H. J. Wallbaum, *Z. Angew. Mineral.*, 1942, **4**, 17–46.

- 34 H. Bärnighausen, *Commun. Math. Chem.*, 1980, **9**, 139–175.
- 35 T. Balić Žunić and E. Makovicky, *Acta Crystallogr., Sect. B: Struct. Sci.*, 1996, **52**, 78–81.
- 36 E. Makovicky and T. Balić-Žunić, *Acta Crystallogr., Sect. B: Struct. Sci.*, 1998, **54**, 766–773.
- 37 U. Betke, K. Neuschulz and M. S. Wickleder, *Chem. – Eur. J.*, 2011, **17**, 8538–8541.
- 38 M. S. Wickleder, *Z. Anorg. Allg. Chem.*, 2000, **626**, 621–622.
- 39 T. Steiner, *Angew. Chem., Int. Ed.*, 2002, **41**, 48–76.
- 40 R. D. Shannon, *Acta Crystallogr., Sect. A: Cryst. Phys., Diffr., Theor. Gen. Crystallogr.*, 1976, **32**, 751–767.
- 41 R. Hoppe, *Angew. Chem.*, 1966, **78**, 52–63.
- 42 R. Hoppe, *Angew. Chem., Int. Ed.*, 1970, **9**, 25–34.
- 43 R. Hübenthal, *MAPLE. Program for the Calculation of the Madelung Part of Lattice Energy*, Universität Gießen, 1993.
- 44 R. A. Zehnder, C. S. Wilson, H. T. Christy, K. S. Harris, V. Chauhan, V. Schutz, M. Sullivan, M. Zeller, F. R. Fronczek, J. A. Myers, K. Dammann, J. Duck, P. M. Smith, A. Okuma, K. Johnson, R. Sovesky, C. Stroudt and R. A. Renn, *Inorg. Chem.*, 2011, **50**, 836–846.
- 45 R. Pascard and C. Pascard-Billy, *Acta Crystallogr.*, 1965, **18**, 830–834.
- 46 M. Amri, N. Zouari, T. Mhiri, S. Pechev, P. Gravereau and R. von der Muhll, *J. Phys. Chem. Solids*, 2007, **68**, 1281–1292.
- 47 C. Postmus and J. R. Ferraro, *J. Chem. Phys.*, 1968, **48**, 3605–3611.
- 48 S. K. Kurtz and T. T. Perry, *J. Appl. Phys.*, 1968, **39**, 3798–3813.
- 49 W. T. Carnall, P. R. Fields and K. Rajnak, *J. Chem. Phys.*, 1968, **49**, 4447–4449.
- 50 T. Kano, in *Phosphor handbook*, ed. H. Yamamoto, S. Shionoya and W. M. Yen, CRC Press, Boca Raton, FL, London, 2nd edn, 2007.
- 51 P. Netzsch, M. Hämmer, P. Gross, H. Bariss, T. Block, L. Heletta, R. Pöttgen, J. Bruns, H. Huppertz and H. A. Höpfe, *Dalton Trans.*, 2019, **48**, 4387–4397.
- 52 C. Peng, C. Li, G. Li, S. Li and J. Lin, *Dalton Trans.*, 2012, **41**, 8660–8668.
- 53 M. W. Nathans and W. W. Wendlandt, *J. Inorg. Nucl. Chem.*, 1962, **24**, 869–879.